Direct and Collateral Alterations of Functional Cortical Circuits in a Rat Model of Subcortical Band Heterotopia

Fanny Sandrine Martineau, Vanessa Plantier, Francoise Watrin, Emmanuelle Buhler, Fanny Sandrine Martineau, Surajit Sahu, Jean-Bernard Manent, Ingrid Bureau, Alfonso Represa

ORIGINAL ARTICLE

Direct and Collateral Alterations of Functional Cortical Circuits in a Rat Model of Subcortical Band Heterotopia

Vanessa Plantier, Françoise Watrin, Emmanuelle Buhler,
Fanny Sandrine Martineau, Surajit Sahu, Jean-Bernard Manent [ID] ,
Ingrid Bureau and Alfonso Represa

INMED, Aix-Marseille Université, INSERM UMR1249, Marseille 13009, France

Address correspondence to Alfonso Represa and Ingrid Bureau, Institut de Neurobiologie de la Méditerranée, INSERM UMR 1249, Parc Scientifique de Luminy – BP13, 163 Avenue de Luminy, 13273 Marseille Cedex 09, Email: alfonso.represa@inserm.fr (A.R.); ingrid.bureau@inserm.fr (I.B.)

Ingrid Bureau and Alfonso Represa are Co-last authors

Abstract

Subcortical band heterotopia (SBH), also known as double-cortex syndrome, is a neuronal migration disorder characterized by an accumulation of neurons in a heterotopic band below the normotopic cortex. The majority of patients with SBH have mild to moderate intellectual disability and intractable epilepsy. However, it is still not clear how cortical networks are organized in SBH patients and how this abnormal organization contributes to improper brain function. In this study, cortical networks were investigated in the barrel cortex in an animal model of SBH induced by *in utero* knockdown of Dcx, main causative gene of this condition in human patients. When the SBH was localized below the Barrel Field (BF), layer (L) four projection to correctly positioned L2/3 pyramidal cells was weakened due to lower connectivity. Conversely, when the SBH was below an adjacent cortical region, the excitatory L4 to L2/3 projection was stronger due to increased L4 neuron excitability, synaptic strength and excitation/inhibition ratio of L4 to L2/3 connection. We propose that these developmental alterations contribute to the spectrum of clinical dysfunctions reported in patients with SBH.

Key words: barrel field, cortical connectivity, electrophysiology, excitability. L4 inputs, subcortical band heterotopia

Introduction

Gray matter heterotopia (GMH) is a group of neurological disorders resulting from abnormal neuronal migration or abnormal positioning and proliferation of neural progenitors (reviewed in Bahi-Watrin et al. 2015). They are characterized by the presence of ectopic clusters of neurons along the ventricular walls (periventricular nodular heterotopia) or in the white matter (subcortical heterotopia and subcortical band heterotopia [SBH]) which is also called double cortex. GMHs are at the origin of hampering symptoms including refractory epilepsy and intellectual disability, with alterations ranging from mild to profound (Dobyns 2010; Guerrini and Dobyns 2014). However, despite the medical and familial impact of GMHs, the pathophysiological bases of clinical manifestations remain poorly understood.

Although the neurons retained in the SBH were destined to populate the overlying cortex, the typical 6-layer cytoarchitectonic organization of this normotopic cortex appears normal in a large population of patients (~28% of cases) (reviewed in Bahi-Buisson et al. 2013) and it is the same in relevant animal models of SBH like Dcx knockdown (Dcx-KD) (Bai et al. 2003) and Tish (Schottler et al. 2001) rats. Interestingly, functional imaging investigations performed on a restricted number of patients suggest that GMHs are associated with reorganizations of cortical representations (Richardson et al. 1998; Pinard et al. 2000; Spreer et al. 2001; Jirsch et al. 2006; Vitali et al. 2008). These authors reported a more widespread activation of the normotopic cortex as compared with control subjects and even in some patients the recruitment of the cortex beyond the limits of the

malformation (Richardson et al. 1998; Vitali et al. 2008). Although the interpretation of these data is hampered by the small number of cases, the variability in the characteristics of heterotopia (e.g., size and localization) and limitations of functional imaging techniques, these data strongly support a link between GMHs and altered organization of cortical circuits. In addition, neurons in the overlying normotopic cortex in SBH animal models display a significant increase in spontaneous glutamatergic synaptic currents (Zhu and Roper 2000; Ackman et al. 2009) and a reduction in GABAergic inhibition (Zhu and Roper 2000; Trotter et al. 2006).

In this report, we seek to evaluate whether SBH affects the organization of functional connections in the barrel field of the primary somatosensory cortex, a classical model to study developing cortical circuits. We used a novel rat model of SBH (Sahu et al. 2016 and in preparation), that we generated by combining RNAi-mediated knockdown of Dcx (Dcx-KD), the main causative gene of SBH (des Portes et al. 1998; Gleeson et al. 1998), with *in utero* electroporation using a triple electrode configuration enabling simultaneous transfection of the 2 brain hemispheres. These Dcx-KD rats develop bilateral SBH that localize in the white matter either below the barrel field of primary somatosensory cortex or below a cortical area lateral to the barrel field, depending on the position of the electrodes used for electroporating RNAi constructs. We took advantage of these inter-individual differences in SBH localization to evaluate the specific impact of SBH position on the organization of functional connections in the rat barrel field, a model system for studying functional cortical circuits. We utilized Laser Scanning PhotoStimulation (LSPS) with glutamate uncaging combined to patch-clamp recordings to map and quantify the strength of functional projections converging onto L2/3 pyramidal neurons in cortical slices from rats (Shepherd et al. 2003). Our data indicate that the presence of subcortical heterotopia below the BF weakens the principal L4 to L2/3 projection in above cortical columns through a decreased connectivity. Opposite outcome is seen when the heterotopia is lateral to the BF. Then, changes in the strength of excitatory L4 to L2/3 synapses, the intrinsic properties of L4 glutamatergic cells and the excitation/inhibition ratio in L2/3 converge into making the early stage of cortical sensory integration abnormally strong, potentially contributing to altered functions of the somatosensory cortex. We therefore propose that developmental changes occur in normotopic cortical networks that could play a major role in the cortical dysfunction of the malformed brain.

Methods

All experiments were performed according to INSERM ethics. This study and protocols were approved by the ethics committee of Ministère de l'enseignement supérieur et de la recherche, France, under the reference 2015040809544569_v2 (APAFIS#436).

Tripolar *In Utero* Electroporation

Tripolar *in utero* electroporation was performed as described by dal Maschio et al. (2012) and by Szczurkowska et al. (2016) with slight modifications. Timed pregnant Wistar rats (Janvier) received buprenorphine (Buprecare at 0.03 mg/kg) and were anesthetized with sevoflurane (4%) 30 min later. Uterine horns were exposed and plasmid vectors (concentration, 1.5 μg/μL) encoding shRNAs targeting the 3′UTR of *Dcx* mRNA or encoding ineffective shRNAs with 3-point mutations creating mismatches (Bai et al. 2003) were microinjected (PV 820 Pneumatic

PicoPump; World Precision Instruments, Sarasota, FL) bilaterally into the lateral ventricles of embryonic day (E) 16 embryos, together with fast green dye and reporter constructs encoding GFP (concentration, 0.5 μg/μL). Reporter constructs expressing GFP were used for visualizing transfected neurons, either found accumulated at ectopic positions and forming SBH, or normally positioned in upper cortical layers (Layers 2–4), consistently with their age of genesis when electroporation is performed. After microinjections, electroporations were accomplished by delivering 50 V voltage pulses (BTX ECM 830 electroporator; BTX Harvard Apparatus, Holliston, MA) across tweezer-type electrodes (Nepa Gene Co, Chiba, Japan) laterally pinching the head of each embryo through the uterus, and a third electrode (patent #WO/2012/153291, inventors: Cancedda L., Ratto G.M., described in dal Maschio et al. 2012 and Szczurkowska et al. 2016) positioned at the brain midline. At birth, successfully electroporated pups were selected after transcranial visualization of the reporter fluorescent proteins. All pups were housed with their mothers until experiments at postnatal day (P) 13 to P16.

Brain Slices Preparation and Electrophysiology

Electroporated rats were used at P13–P16. They were anesthetized with a ketamine/xylazin mix ([65 mg/kg, 6 mg/kg]) prior decapitation. Across-row barrel cortex slices (300 μm thick) were cut with a 45-degree angle from midline and 45-degree angle from the horizontal plane to preserve as much as possible the axons and dendrites of cells (Finnerty et al. 1999; Shepherd and Svoboda 2005). The chilled cutting solution contained (in mM): 110 choline chloride, 25 $NaHCO_3$, 25 D-glucose, 11.6 sodium ascorbate, 7 $MgCl_2$, 3.1 sodium pyruvate, 2.5 KCl, 1.25 NaH_2PO_4, and 0.5 $CaCl_2$. Slices were transferred to artificial CSF (aCSF) containing the following (in mM): 127 NaCl, 25 $NaHCO_3$, 25 D-glucose, 2.5 KCl, 1 $MgCl_2$, 2 $CaCl_2$, and 1.25 NaH_2PO_4, aerated with 95% O_2 and 5% CO_2, first at 34°C for 15 min and then at room temperature before use. Slices illuminated with infrared light were inspected with a 4× and a 60× objective in order to position the recording pipettes in distinct layers. L4 had barrel-like structures. L5A was a clear band below L4 and above a denser L5B. Pyramidal cells in L2/3 were patched using borosilicate electrodes (4–6 MΩ). The intracellular solution contained the following (in mM): 128 CsMeS, 10 HEPES, 10 Sodium PhosphoCreatine, 4 $MgCl_2$, 4 NaATP, 0.4 NaGTP, 3 Ascorbicacid. Whole-cell recordings were made using a Multiclamp 700 A (Molecular Devices, Sunnyvale, CA) amplifier. Cells were identified based on their laminar and columnar positions. EPSCs were measured in whole-cell configuration at −70 mV, near the reversal potential of GABAergic conductances, and IPSCs at 0 mV, near the reversal potential of glutamate conductances. L4 cells were recorded in loose-seal configuration to record action potentials (APs). Custom software for instrument control and acquisition was written in Matlab (Mathworks, Natick, MA).

Laser Scanning PhotoStimulation with Glutamate Uncaging

Laser Scanning PhotoStimulation (LSPS) was performed as described by Bureau et al. (2008). Recirculating aCSF solution contained the following (in mM): 0.37 NI (nitroindolinyl)-caged glutamate (Canepari et al. 2001) (Tocris Bioscience), 0.005 CPP [()-3-(2- carboxypiperazin-4-yl)propyl-1-phosphonic acid] (NMDA receptors antagonist, Sigma Aldrich), 4 $CaCl_2$, and 4 $MgCl_2$. Traces of whole-cell voltage-clamp recordings were sampled and filtered

at 10 kHz. Focal photolysis of caged glutamate was accomplished with a 2-ms 20 mW pulse of a UV (355 nm) laser (DPSS Lasers Inc.) through a 0.16 NA 4 × objective (Olympus). The standard stimulus pattern for LSPS mapping consisted of 324 positions on an 18 × 18 grid (spacing = 75 μm). The slice was oriented so that the pia was on the top and the barrels A to E were aligned horizontally from left to right. The laser was moved in a spatial pattern designed to avoid consecutive glutamate uncaging over neighboring pixel sites (Shepherd et al. 2003). LSPS was also used to quantify the generation of spikes in neurons. Excitation profiles of L4 cortical cells were recorded in loose-seal configuration while uncaging glutamate over a smaller grid (centered on the soma, 8 × 8 grid, spacing = 50 μm). Recordings were performed in columns corresponding to the B or C whiskers.

Analysis of LSPS Maps

Synaptic input maps for individual neurons were constructed by computing the mean current amplitude calculated in a 100-ms time window 7-ms after the UV stimulus for each position of photostimulation. Typically, 2–4 maps were obtained per cell and averaged. Synaptic and direct responses were distinguished based on their latencies. Sites where stimulation evoked direct responses were close to the recording site and were excluded from the analysis. Averaged single-cell maps were used to compute group-averaged maps. Interpolation was performed on averaged synaptic input maps for display purposes. Traces of loose-seal recordings were analyzed for APs. A spatial profile of excitability (excitation profile) was generated by plotting the number of APs elicited at each uncaging site in a 100-ms time window immediately after the stimulus. All values are given as means ± SEM. Statistical analyses were performed using GraphPad Prism 5. All P values for Figure 2 refer to two-way ANOVA test and Dunnett's multiple comparison post-test. For Figures 3, 5D and 6, P values refer to Kruskal–Wallis test, unless noted otherwise. For Figure 4, P value refers to Spearman test. For Figure 5G, P value refers to Mann–Whitney test.

Minimal Stimulations

After patching the L2/3 cell, glutamate was uncaged 15–25 times every 15 s in L4, at a site where one of the largest responses was detected in an LSPS input map. The laser power was lowered until 1 or 2 unitary postsynaptic currents (uPSCs) of constant amplitude were seen repeatedly with detectable failure rates (10–20%). These failures were attributable to failures in evoking APs in L4 cells (Bureau et al. 2008). The uPSC were selected manually and detection threshold for events was set at 6 pA, about 2 times the noise standard deviation (Mismatch, 2.9 ± 0.1 pA; SBH below BF, 3.5 ± 0.2 pA; SBH lateral to BF, 3.0 ± 0.2 pA). Amplitudes of uPSCs were averaged per L4 to L2/3 connection.

Histology

Slices from brains of all analyzed rats were fixed with paraformaldehyde (4% in phosphate-buffered saline [PBS]). Slices were permeabilized for 1 h at room temperature in PBS–Triton X-100 (0.1%) - goat serum (5%). After permeabilization, revelation of biocytin-injected neurons was obtained with Alexa 555-conjugated streptavidin (1:500; Millipore Bioscience Research Reagents) for staining of transfected cells. Sections were examined under a Zeiss laser-scanning microscope (Zeiss LSM800)

using 5x and 20x objectives. Images were digitized using the built-in software (ZEN 2) and exported in tiff format.

Results

Inter-Individual Differences in SBH Position in Dcx-KD Rats

The main objective of our study was to investigate the functional organization of cortical circuits in brains with SBH. To this purpose, we studied a rat model of SBH (Sahu et al. 2016 and in prep), that we generated by *in utero* electroporation with RNAi-mediated knockdown of *Dcx*, the main causative gene of SBH in human patients (Gleeson et al. 1998; des Portes et al. 1998). *In utero* electropration was performed at E16 leading to a Dcx knockdown in developing upper layer neurons (L4, L2/3). These rats present with bilateral SBH resembling those seen in human patients, and develop spontaneous epileptic manifestations after the age of 2 months (Sahu et al. 2016 and in preparation). Here, we studied these rats at P13–P16, when projections to L2/3 were developing (Bureau et al. 2004) and before animals showed signs of epilepsy.

We cut brain slices so as to preserve circuit organization in the BF (Finnerty et al. 1999). Visual inspection of slices revealed that SBH position in the white matter varied from below the BF to below the adjacent motor areas (Fig. 1), likely depending on the position of electrodes used for electroporating RNAi constructs. We took advantage of this inter-individual difference to evaluate separately the effects of SBH on circuit organization of functional connections impinging onto pyramidal cells that were correctly positioned in L2/3 of the BF. To this purpose, we categorized 2 different situations according to the position of SBH relative to BF (Fig. 1): either the SBH extended directly below the recorded cortical columns corresponding to whiskers B and C of the BF (n = 11 rats) or it localized lateral to the medial boundary of the recorded columns (see Methods) (n = 17 rats). Our control situation corresponded to rats electroporated with ineffective RNAi constructs (mismatch), and harboring no SBH (n = 11 rats).
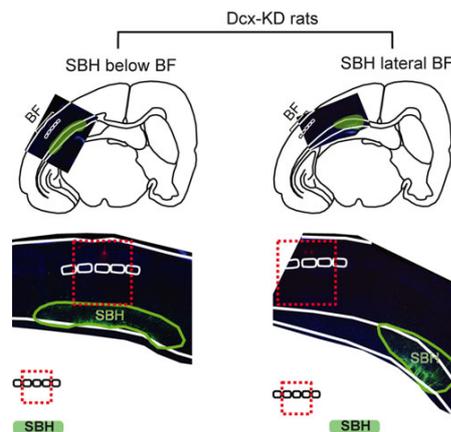

Figure 1. Representative examples of across-barrel brain slices in Dcx-KD rats highlighting inter-individual differences in subcortical band heterotopia (SBH) positions. Fluorescence microphotographs are superimposed on schematized views of across-barrel slices for illustrating the position of SBH relative to the barrel field (BF). Red dashed line rectangles illustrate the cortical columns of interest for mapping. Red point into the slice represents the cell labeled with biocytin and recorded in electrophysiological experiments (Columns B or C).
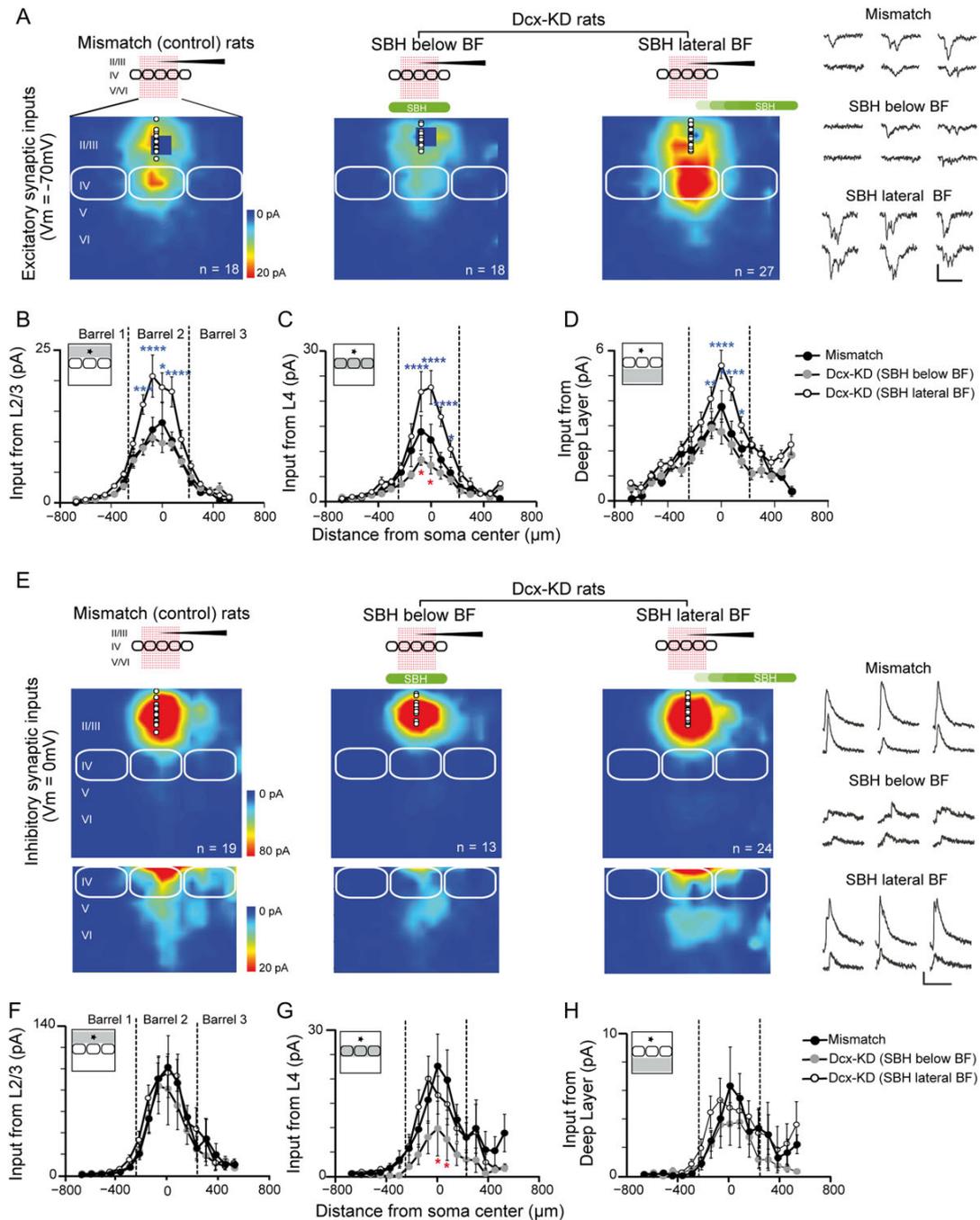
Figure 2. Excitatory and inhibitory synaptic input maps for L2/3 neurons in mismatch and Dcx-KD rats. (A) Cells were recorded in L2/3 (holding: −70 mV) and the 18 × 18 uncaging grid stimulated 3 cortical columns of the barrel field (BF), from L2 to L6. Colors indicate the mean amplitude of excitatory synaptic responses in a 100-ms time window. White circles show soma positions of recorded L2/3 neurons. Solid white lines delineate barrels. Synaptic responses evoked at blue pixels close to recording sites were masked by direct glutamate-evoked responses and could not be analyzed. Examples traces of synaptic currents recorded in L2/3 cells and evoked by stimulating the L4 are shown for each group at the right. Scale bars are 50 pA and 100 ms. (B) Horizontal profile (75 μm bins) of L2/3 excitatory inputs as a function of distance with soma in mismatch (black) and Dcx-KD rats (gray, the SBH is below the BF; open symbols, the SBH is lateral to the BF). The gray area in maps shown in inset indicates the region of analysis. (C) Same as in B for L4 excitatory inputs. (D) Same as in B for L5/6 excitatory inputs. (E F G H) Same as in A B C D for inhibitory synaptic inputs recorded in L2/3 pyramidal cells at 0 mV membrane potential. Examples traces of synaptic currents recorded in L2/3 cells and evoked by stimulating the L4 are shown for each group at the right. Scale bars are 50 pA and 100 ms. Two-way ANOVA, Dunnett's multiple comparisons test, *$P < 0.05$, **$P < 0.01$, ****$P < 0.001$.
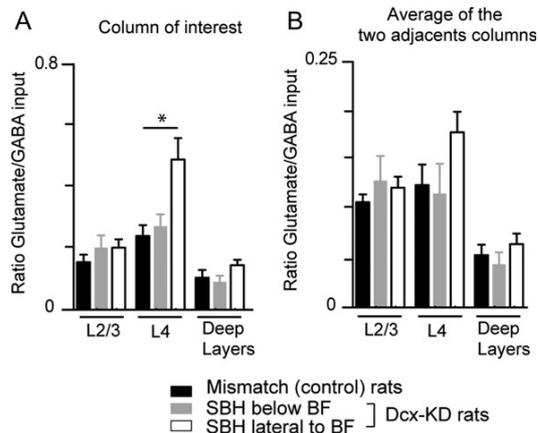
Figure 3. Comparison between excitatory and inhibitory inputs on L2/3 neurons in mismatch and Dcx-KD rats. Excitatory/inhibitory input ratios in L2/3 neurons upon glutamate uncaging in L2/3, L4, and deep layers in mismatch and Dcx-KD rats. The excitatory/inhibitory input ratio from L4 of the same column (A) is significantly increased when the SBH is lateral to the barrel field (BF). No changes were observed for projections originating in adjacent columns (B). (Kruskal–Wallis test, *P < 0.05).

Excitatory and Inhibitory Synaptic Inputs onto L2/3 Neurons are Differentially Altered Depending on SBH Position

To map the functional excitatory and inhibitory projections to L2/3 neurons in brain slices (Fig. 2), we used LSPS coupled with caged glutamate (Shepherd et al. 2003; Bureau et al. 2004, 2008). Glutamate was photo-released on the focal spot of a UV laser beam on an 18 × 18 pixel grid to excite cells of different layers while a L2/3 pyramidal cell was recorded in voltage-clamp mode. EPSCs were isolated by holding membrane potential of L2/3 neurons at −70 mV (Fig. 2A) and IPSCs by holding membrane potential at 0 mV (Fig. 2E). Recordings were performed in columns corresponding to the B and C whiskers.

Excitatory L2/3 to L2/3 projections increased strength in Dcx-KD rats (n = 27 cells) compared with mismatch (n = 18 cells) when the SBH was localized lateral to the recorded cortical columns (Fig. 2B). However, this strength did not change when the SBH was located below the BF (n = 18 cells). Excitatory L4 to L2/3 projections were altered in Dcx-KD rats when compared with mismatch but the type of change differed dramatically depending on the position of the SBH (Fig. 2C): when the SBH was below the BF, synaptic inputs were depressed, particularly at the center of the barrel; when SBH was lateral to the BF, synaptic inputs were potentiated. Excitatory L5 to L2/3 cell projections strengthened in Dcx-KD rats too when SBH was lateral to the BF (Fig. 2D).

Inhibitory projections from any input region (L2/3, L4, and L5) were unchanged in Dcx-KD rats compared with mismatch (n = 19) when the SBH was lateral to the BF (n = 24; Fig. 2F–H). However, inhibitory L4 to L2/3 projection was depressed when the SBH was below the BF (n = 13, red star, Fig. 2G).

Above results suggest that excitatory inputs to L2/3 were potentiated when the SBH was localized lateral to the BF and that excitatory and inhibitory synaptic projections to L2/3 neurons were depressed when the SBH was localized below the BF. To evaluate if these changes had consequences on functional synaptic integration, we analyzed the mean amplitude for excitatory and inhibitory inputs to L2/3 from each region of the normotopic cortex (Supplementary Table S1) and we studied the ratio between the excitation and inhibition received by L2/3 cells. The glutamate/GABA ratios for the projections originating in L2/3, L4, and deep layers of the same column were similar in mismatch and Dcx-KD rats when the SBH was localized below the BF (Fig. 3A). However, this ratio increased significantly for projections originating in L4 when the SBH localized lateral to the BF (P < 0.05, Fig. 3A). We did not observe any change for projections originating in adjacent columns (Fig. 3B).

The Strength of L4 to L2/3 Projections is Correlated with the Size and Position of Subcortical Band Heterotopia in the Slice

The distance separating the recorded neuron from the malformation was different for each animal. We found that the Dcx-KD group of rats with SBH lateral to BF could be further divided (Fig. 4A) so that a gradient of effect was now observed between L4 inputs and SBH position (Fig. 4B). L4 inputs were stronger when SBH was totally excluded from the BF area in the slice. They displayed an intermediate strength when the SBH was localized under other cortex and extended to the most medial portion of the BF, adjacent to the columns recorded. Finally, they were weaker when the SBH localized directly below the columns recorded in the BF (Fig. 4B).

In addition of having variable positions, SBH had different sizes from 0.088 to 0.615 mm² (mean value was 0.39 ± 0.19 mm², measured in the recorded slice). We found that when the SBH was completely out of the BF area in the recorded slice, the amplitude of L4 inputs to L2/3 increased in a correlative manner with the size of malformation (Spearman r = 0.83, n = 11, P < 0.01; Fig. 4C, D). We also noticed that the SBH must have a minimal size (>0.2 mm²) in order to see this potentiation. No correlation was observed when the SBH were in the BF area (Spearman r = 0 for SBH under BF, n = 9; Spearman r = 0.26 for SBH intermediate, P > 0.05, n = 7).

Overall, these results suggest that the functional organization of cortical circuits is altered in brain with SBH, with interindividual differences related to the precise location and size of SBH.

Increased Excitability of L4 Neurons When SBH is Out the Barrel Field

We next studied if the change in the ascending L4 to L2/3 projection in Dcx-KD rats when the SBH localized out of the BF was due to an increase of L4 cell excitation evoked by LSPS. To evaluate L4 cell excitation, we recorded AP in loose-seal configuration (Shepherd and Svoboda 2005; Bureau et al. 2008). Glutamate was uncaged on an 8 × 8 grid centered on the patch pipette (Fig. 5A). Glutamate-evoked excitation was similar in mismatch and Dcx-KD rats when SBH was below the BF (Fig. 5B–D; n = 19 and 16, respectively). Then, L4 cells fired about 1 AP when glutamate was uncaged above or close to the soma. Firing increased to about 2 AP per site in slices where SBH was out of the BF (n = 12 cells; Fig. 5B–D). Interestingly, the glutamate-evoked excitation was intermediate when the SBH was in the BF but on the side of the investigated column (n = 8 cells, mean = 1.5 AP/site). These data suggest that intrinsic properties of L4 cells change depending on the position of the SBH.

We studied this hypothesis with whole-cell recording experiments in which firing activity was measured with the injection of steps of depolarizing current (Fig. 5E). Firing rate
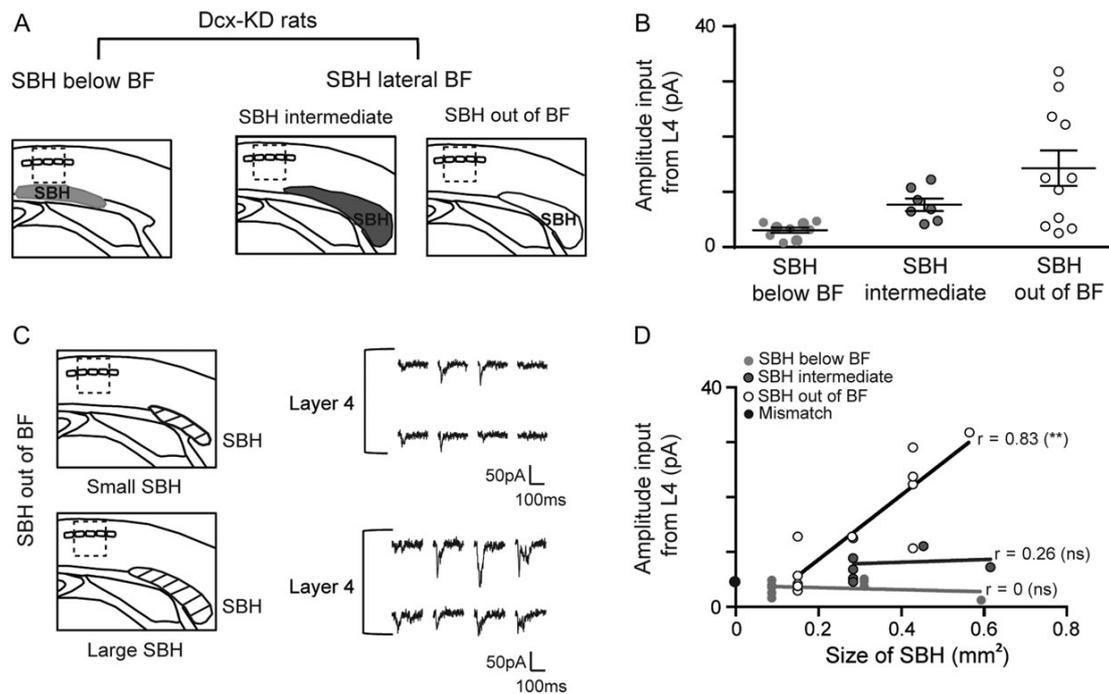
Figure 4. Correlation between amplitude of excitatory inputs from L4 to L2/3 neurons and the position and size of subcortical band heterotopia (SBH) in the slice. (A) Drawings illustrating the different positions of the SBH compared with Barrel Field (BF). (B) Change in amplitude of L4 excitatory inputs depends on the position of the SBH in cortex. (C) Traces on the right show synaptic responses evoked by glutamate uncaging at 8 sites in L4, as recorded in L2/3 neuron from 2 Dcx-KD rats with a small (top) or large (bottom) SBH drawn in left panels. (D) The amplitude of excitatory inputs from L4 is correlated with the size of the SBH in Dcx-KD rats when the SBH is out of the BF (open symbols, Spearman test, **P < 0.01) but not when the SBH is below the recorded columns (light gray) or below adjacent columns of the BF (dark gray). In mismatch rats with no SBH, the mean amplitude of L4 input is around 6pA (black symbol).

was larger in Dcx-KD when the SBH was out of the BF for every step of currents tested (100–300 pA, $n = 6$ cells) compared with when the SBH was below the BF ($n = 14$ cells; Fig. 5F). Furthermore, the membrane threshold above which AP was elicited was lower by 6 mV in cases SBH was out of the BF ($P < 0.01$, Mann–Whitney test, Fig. 5G). Altogether, these results suggest a hyperexcitability of L4 cells in barrels lateral to the malformation that could account for the brighter LSPS input maps described earlier.

Increased Synaptic Strength in L2/3 Cells of Dcx-KD Rats When the SBH is Out of the BF

Another mechanism that could contribute to the strengthening of L4 to L2/3 projection is an increase of synaptic strength. We measured the strength of the synaptic connection in pairs of L4–L2/3 connected cells with a LSPS-based minimal stimulation protocol (Bureau et al. 2008). For each pyramidal cell recorded in L2/3, glutamate was uncaged at low frequency at 1 site in L4 that evoked a robust response. Then, laser power was decreased until each stimulus evoked a single EPSC of constant amplitude or none in the postsynaptic cell (Fig. 6A; see Methods). Under these conditions, each EPSC corresponded to the stimulation of a single presynaptic cell firing 1 AP. Amplitudes of unitary events (I_{uni}) were similar in mismatch rats and in Dcx-KD rats with a SBH below the BF (16 ± 5 pA, $n = 17$ and 16 ± 8 pA, $n = 11$, respectively; Fig. 6B). However, amplitude increased significantly when the SBH was located out of the BF (27 ± 13 pA, $n = 13$, $P < 0.05$; Fig. 6B).

Thus, the stronger L4 to L2/3 projections observed in LSPS maps of rats with a SBH lateral to the BF could be explained by stronger synapses and hyperexcitability of L4 cells. In contrast, the lack of difference in the size of unitary events, AP discharge and intrinsic excitability suggest the weaker L4 to L2/3 projections observed in LSPS maps of rats with a SBH below the BF was due to lower connectivity.

Discussion

In this study, we evaluated the functional intracortical organization of the BF in presence of a malformation. In our rat model, SBH has variable size and position in the white matter that resembled clinical descriptions of heterotopia in patients with double-cortex. We found the spectrum of changes observed in Dcx-KD rats could be categorized in 2 main categories: one occurring when the normotopic cortex is located above the SBH and the other occurring when the normotopic cortex is located laterally to the SBH. The presence of the SBH below the BF led to a weakening of excitatory and inhibitory projections impinging onto L2/3 pyramidal cells which soma was located in the above normotopic cortex. In contrast, the presence of the SBH in the adjacent cortical area led to a strengthening of these excitatory projections.

Changes in the Cortex Above the Heterotopia

In Dcx-KD rats, we found that L4 to L2/3 excitatory projection was 50% weaker when the SBH was located below the BF. This was likely caused by a decrease in connectivity because other
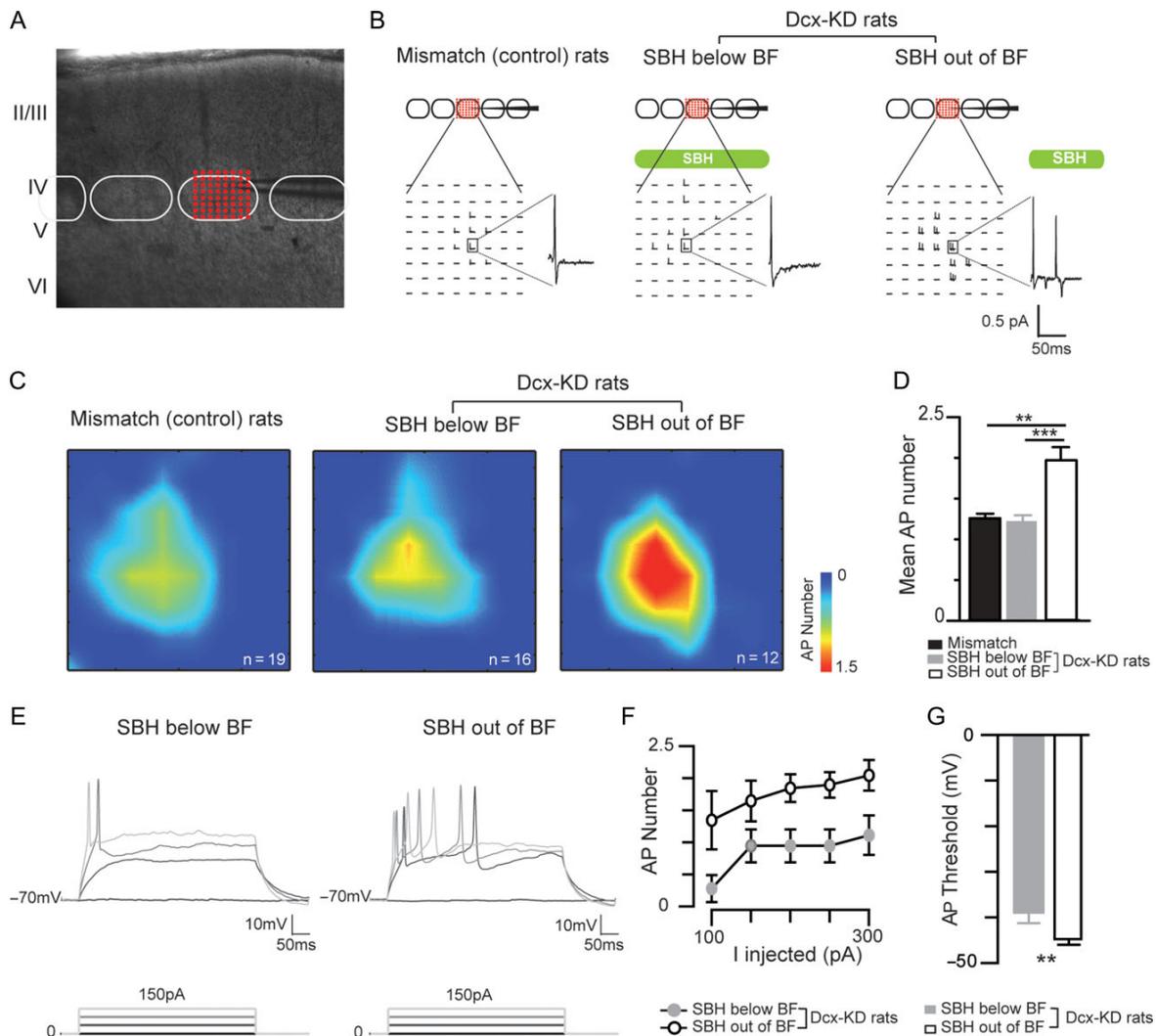
Figure 5. L4 neurons are hyperexcitable in Dcx-KD rats when the Subcortical Band Heterotopia (SBH) is located out of the Barrel Field (BF). (A) Illustration of the protocol. The cell recorded in loose patch configuration is in L4, at the center of a 8×8 uncaging grid. (B) Examples of photostimulation-evoked action potential (AP) elicited over the 8×8 uncaging grid in L4 neurons from mismatch and Dcx-KD rats. APs are shown enlarged for each condition. (C) Excitation profiles averaged across L4 neurons in mismatch and Dcx-KD rats. Number of action potentials (APs) is color-coded. (D) Number of evoked APs in mismatch and Dcx-KD rats. **$P < 0.01$, ***$P < 0.001$, Kruskal–Wallis test. (E) Discharges in L4 cells from 2 Dcx-KD rats with a SBH below the recorded cells (left) or out of the BF (right) evoked by steps of depolarizing currents. (F) Number of APs evoked by increasing steps of depolarizing currents in L4 cells of Dcx-KD rats. (G) AP threshold recorded in L4 cells of Dcx-KD rats. Mann–Whitney test, **$P < 0.01$.

investigated cellular parameters (i.e., synaptic strength and L4 excitability) were stable. Since neurons forming the SBH do not reach the L4–L2/3 upper cortical layers to which they were destined, these layers may have a neuronal depletion which could explain the weaker L4 to L2/3 excitatory projection. However, depletion of cells should lead to the development of stronger synaptic connections as observed *in vitro* (Ivenshitz and Segal 2010), which does not occur in our rat model. Anatomical investigations are needed to resolve this issue. Another hypothesis is that the lower density of L4 to L2/3 connections is a consequence of perturbations that occurred at an earlier stage of sensory integration, at the level of thalamocortical projection in L4, which would deprive cortex from normal sensory inputs and alter development of circuits (Erzurumlu and Gaspar 2012).

Note that barrels were still visible in Dcx-KD rats, an observation inconsistent with a complete loss of thalamic inputs. Nevertheless, the SBH might either partially prevent the penetration of thalamic axons into the cortex or alter the functional consolidation of thalamocortical synapses. Clinical evidences are contradictory at this point. Investigations of fiber bundles in patients with a SBH using diffusion-tensor imaging and fiber tractography described indeed a disorganization of the main axonal tracts (Lee et al. 2005; Lu et al. 2008; Iannetti et al. 2011). But another study described similar patterns of connectivity in patients and controls, with tracts that appeared to cross or end within the band heterotopia (Eriksson et al. 2002). Variability in heterotopic bands between subjects could reconcile these findings (Lu et al. 2008). Another important feature to consider is
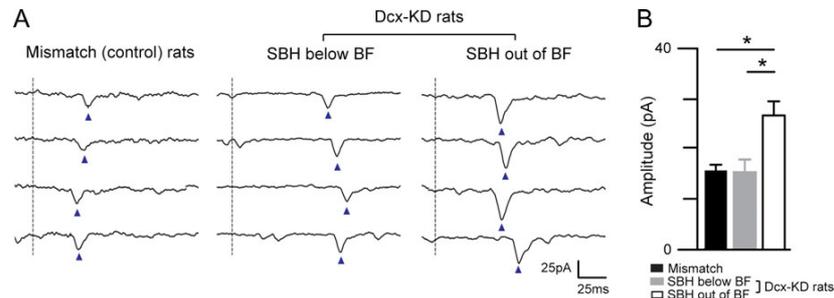
Figure 6. Strength of single L4 to L2/3 connections is enhanced when Subcortical Band Heterotopia (SBH) is located out the Barrel Field (BF). (A) Traces are examples of unitary events evoked by minimal stimulation in L4 and recorded in L2/3 pyramidal cell in a mismatch rat (left), and in 2 Dcx-KD rats with a SBH either below (middle) or out of the BF (right). Vertical dashed lines indicate time of photostimulus. Arrowheads show unitary events evoked by stimulations of same presynaptic L4 neuron across trials. (B) Amplitude of unitary events in mismatch and Dcx-KD rats. Kruskal–Wallis test, *$P < 0.05$.

the contribution of ectopic neurons to cortical function. Indeed, functional MRI studies have shown that the SBH is also activated during the completion of sensory tasks (Richardson et al. 1998; Spreer et al. 2001; Villani et al. 2004; Wennberg et al. 2004; Jirsch et al. 2006; Vitali et al. 2008). Interestingly, research on Tish rats, a model of double-cortex caused by a spontaneous mutation in Eml1 (Grosenbaugh et al. 2017), showed that stimulation of single whisker increased activity of both normotopic and heterotopic neurons (Schottler et al. 2001). Hence, 2 whisker maps could co-exist, one in the normotopic cortex, the other in the SBH, and that the decreased strength of intracortical circuits in the normotopic cortex would result from a dispersion of afferent inputs in the 2 different target areas. These hypotheses could be tested with the study of the functional properties and topography of thalamocortical connections in the diseased cortex.

Changes in the Cortex Lateral to the SBH

Changes in projections impinging onto L2/3 pyramidal cells were entirely different when the SBH was out of BF. L4 to L2/3 excitatory projection was strengthened by a factor of 2 due to an increased excitability of L4 cells and a strengthening of L4 to L2/3 synapses. No change was detected in inhibition suggesting the overall outcome for barrel cortex of the presence of SBH in the adjacent cortex was an increased drive of L2/3 cells upon stimulation. It is important to note that the cortex localized adjacent to the BF is the motor cortex. Sensory and motor cortices operate in close interaction as evidenced by anatomical and functional studies (White and DeAmicis 1977; Porter and White 1983; Deschenes et al. 1998; Ferezou et al. 2007). Interactions begin at an early developmental stage when pups have few voluntary movements while they are already treating somatosensory information crucial to their survival. Then, the motor area is said to operate in a "sensory mode" (Khazipov and Milh 2018) and its activation follows the occurrence of spontaneous movements (or twitches) (McVea et al. 2012; Tiriac et al. 2014). The strengthening of circuits in the BF of Dcx-KD rats could correspond to compensating mechanism activated by alterations affecting motor cortex. This would allow functions normally assigned to the young motor cortex to be undertaken by neighboring circuits (Bittar et al. 2000; Bruurmijn et al. 2017). Alternatively, plasticity in the BF could also correspond to a consolidation of spared functions in a partially deprived cortex. There is indeed a mechanistic parallel to be made between the potentiating effects we describe in Dcx-KD rats and the effects obtained with partial sensory deprivation which include a

potentiation of excitatory synapses (Finnerty et al. 1999; Clem and Barth 2006) and a reduction of the inhibitory drive (Gambino and Holtmaat 2012) in cortical columns next to a "deprived column".

Functional Disorganization and Clinical Manifestations

It is unclear at present if patients with SBH display alterations in cortical areas next to the lesion as most functional studies were dedicated to identifying epileptogenic focus. However, the analysis of interictal spikes with EEG combined with functional MRI helps identifying functional networks. In the large majority of patients with a SBH, activation was detected in the heterotopia and the surrounding cortex (Mai et al. 2003; Tassi et al. 2005; Kobayashi et al. 2006; Tyvaert et al. 2008; Pizzo et al. 2017). The analysis of BOLD (Blood oxygenation level-dependent) signals identified a concomitant involvement of distal sites (Kobayashi et al. 2006) in the majority of these analyses. Similar observations have been reported in patients with periventricular nodular heterotopia (Valton et al. 2008; Christodoulou et al. 2012; Shafi et al. 2015; Pizzo et al. 2017). Interestingly, imaging analysis of patients with cortical malformations, including patients with a SBH, revealed signs of cortical functional reorganization beyond visible lesion boundaries (Richardson et al. 1998; Pinard et al. 2000; Spreer et al. 2001; Jirsch et al. 2006; Vitali et al. 2008), and it was proposed that activation of wider cortical areas indicates the need for a widespread network to perform simple tasks (Richardson et al. 1998, Jirsch et al. 2006). Our data demonstrating a functional reorganization of the cortex lateral to the SBH in animals before epilepsy onset, would provide a rationale for the changes observed in patients. Moreover, the observation that the SBH must have a minimal size below motor cortex in order to see significant changes in the BF (Fig. 4D) is aligned with clinical observations that epilepsy severity and the size of heterotopia are linked (Bahi-Buisson et al. 2013). We propose that band heterotopia formation leads to a secondary functional reorganization of the adjacent cortex which increases its excitation that subsequently contributes to the generation of epileptic networks. It will be important to further charaterize this sequence of events in order to better define epileptogenic foci and propagation pathways.

Other types of cortical malformations might lead to similar consequences. Investigations of a rat model of microgyria induced by freeze-lesioning of deep layer neurons at neonatal stage demonstrated that limb and trunk somatosensory areas, 0.5–1 mm lateral to the microgyria, displayed an increased excitation in L5 and an increased inhibition in L5 and L2/3 (Jacobs

and Prince 2005; Brill and Huguenard 2010; Jin et al. 2014). Differences exist with the Dcx-KD model as for the mechanisms of disruption because freeze lesion did not change the excitability of excitatory neurons and it strengthened inhibitory synapses. There are great differences between the 2 animal models that would explain it. Dcx-KD rats have developmental alteration in which neurons fail to migrate and integrate the overlaying cortex while freeze-lesioned rats experience the destruction of layers already formed and somehow connected. Yet despite divergences in origin and mechanism, the final consequence of both malformations is an increased activation of the adjacent, in appearance sane, cortical area.

Our study indicates that the formation of SBH in Dcx-KD rats induces alteration in cortical network development that would have important functional consequences. Our study demonstrates that the impact of the heterotopia differs with its size and precise position and that not only the overlaying cortex but also the cortex lateral to the heterotopia are modified. Further studies are required for evaluating the impact of these changes on the BF functions.

Supplementary Material

Supplementary material is available at *Cerebral Cortex* online.

Funding

Notes

References

Ackman JB, Aniksztejn L, Crepel V, Becq H, Pellegrino C, Cardoso C, Ben-Ari Y, Represa A. 2009. Abnormal network activity in a targeted genetic model of human double cortex. J Neurosci. 29:313–327.

Bahi-Buisson N, Souville I, Fourniol FJ, Toussaint A, Moores CA, Houdusse A, Lemaitre JY, Poirier K, Khalaf-Nazzal R, Hully M, et al. 2013. New insights into genotype-phenotype correlations for the doublecortin-related lissencephaly spectrum. Brain. 136:223–244.

Bai J, Ramos RL, Ackman JB, Thomas AM, Lee RV, LoTurco JJ. 2003. RNAi reveals doublecortin is required for radial migration in rat neocortex. Nat Neurosci. 6:1277–1283.

Bittar RG, Ptito A, Reutens DC. 2000. Somatosensory representation in patients who have undergone hemispherectomy: a functional magnetic resonance imaging study. J Neurosurg. 92:45–51.

Brill J, Huguenard JR. 2010. Enhanced infragranular and supragranular synaptic input onto layer 5 pyramidal neurons in a rat model of cortical dysplasia. Cereb Cortex. 20:2926–2938.

Bruurmijn M, Pereboom IPL, Vansteensel MJ, Raemaekers MAH, Ramsey NF. 2017. Preservation of hand movement representation in the sensorimotor areas of amputees. Brain. 140: 3166–3178.

Bureau I, Shepherd GM, Svoboda K. 2004. Precise development of functional and anatomical columns in the neocortex. Neuron. 42:789–801.

Bureau I, Shepherd GM, Svoboda K. 2008. Circuit and plasticity defects in the developing somatosensory cortex of FMR1 knock-out mice. J Neurosci. 28:5178–5188.

Canepari M, Nelson L, Papageorgiou G, Corrie JE, Ogden D. 2001. Photochemical and pharmacological evaluation of 7-nitroindolinyl-and 4-methoxy-7-nitroindolinyl-amino acids as novel, fast caged neurotransmitters. J Neurosci Methods. 112:29–42.

Christodoulou JA, Walker LM, Del Tufo SN, Katzir T, Gabrieli JD, Whitfield-Gabrieli S, Chang BS. 2012. Abnormal structural and functional brain connectivity in gray matter heterotopia. Epilepsia. 53:1024–1032.

Clem RL, Barth A. 2006. Pathway-specific trafficking of native AMPARs by in vivo experience. Neuron. 49:663–670.

dal Maschio M, Ghezzi D, Bony G, Alabastri A, Deidda G, Brondi M, Sato SS, Zaccaria RP, Di Fabrizio E, Ratto GM, et al. 2012. High-performance and site-directed in utero electroporation by a triple-electrode probe. Nat Commun. 3:960.

des Portes V, Francis F, Pinard JM, Desguerre I, Moutard ML, Snoeck I, Meiners LC, Capron F, Cusmai R, Ricci S, et al. 1998. Doublecortin is the major gene causing X-linked subcortical laminar heterotopia (SCLH). Hum Mol Genet. 7:1063–1070.

Deschenes M, Veinante P, Zhang ZW. 1998. The organization of corticothalamic projections: reciprocity versus parity. Brain Res Brain Res Rev. 28:286–308.

Dobyns WB. 2010. The clinical patterns and molecular genetics of lissencephaly and subcortical band heterotopia. Epilepsia. 51(Suppl 1):5–9.

Eriksson SH, Symms MR, Rugg-Gunn FJ, Boulby PA, Wheeler-Kingshott CA, Barker GJ, Duncan JS, Parker GJ. 2002. Exploring white matter tracts in band heterotopia using diffusion tractography. Ann Neurol. 52:327–334.

Erzurumlu RS, Gaspar P. 2012. Development and critical period plasticity of the barrel cortex. Eur J Neurosci. 35:1540–1553.

Ferezou I, Haiss F, Gentet LJ, Aronoff R, Weber B, Petersen CC. 2007. Spatiotemporal dynamics of cortical sensorimotor integration in behaving mice. Neuron. 56:907–923.

Finnerty GT, Roberts LS, Connors BW. 1999. Sensory experience modifies the short-term dynamics of neocortical synapses. Nature. 400:367–371.

Gambino F, Holtmaat A. 2012. Spike-timing-dependent potentiation of sensory surround in the somatosensory cortex is facilitated by deprivation-mediated disinhibition. Neuron. 75:490–502.

Gleeson JG, Allen KM, Fox JW, Lamperti ED, Berkovic S, Scheffer I, Cooper EC, Dobyns WB, Minnerath SR, Ross ME, et al. 1998. Doublecortin, a brain-specific gene mutated in human X-linked lissencephaly and double cortex syndrome, encodes a putative signaling protein. Cell. 92: 63–72.

Grosenbaugh DK, Joshi S, Lee KS, Fitzgerald MP, Anzivino MJ, McConnell MJ, Goodkin HP A spontaneous deletion in Eml1 underlies the bilateral cortical malformation in the tish rat model of subcortical heterotopia. Program No 293.03. 2017

Neuroscience Meeting Planner. Washington, DC: Society for Neuroscience, 2017. Online

Guerrini R, Dobyns WB. 2014. Malformations of cortical development: clinical features and genetic causes. Lancet Neurol. 13(7):710–726.

Iannetti P, Nicita F, Spalice A, Parisi P, Papetti L, Verrotti A. 2011. Fiber tractography assessment in double cortex syndrome. Childs Nerv Syst. 27:1197–1202.

Ivenshitz M, Segal M. 2010. Neuronal density determines network connectivity and spontaneous activity in cultured hippocampus. J Neurophysiol. 104:1052–1060.

Jacobs KM, Prince DA. 2005. Excitatory and inhibitory postsynaptic currents in a rat model of epileptogenic microgyria. J Neurophysiol. 93:687–696.

Jin X, Jiang K, Prince DA. 2014. Excitatory and inhibitory synaptic connectivity to layer V fast-spiking interneurons in the freeze lesion model of cortical microgyria. J Neurophysiol. 112:1703–1713.

Jirsch JD, Bernasconi N, Villani F, Vitali P, Avanzini G, Bernasconi A. 2006. Sensorimotor organization in double cortex syndrome. Hum Brain Mapp. 27:535–543.

Khazipov R, Milh M. 2018. Early patterns of activity in the developing cortex: Focus on the sensorimotor system. Semin Cell Dev Biol. 76:120–129.

Kobayashi E, Hawco CS, Grova C, Dubeau F, Gotman J. 2006. Widespread and intense BOLD changes during brief focal electrographic seizures. Neurology. 66:1049–1055.

Lee SK, Kim DI, Kim J, Kim DJ, Kim HD, Kim DS, Mori S. 2005. Diffusion-tensor MR imaging and fiber tractography: a new method of describing aberrant fiber connections in developmental CNS anomalies. Radiographics. 25:53–65.

Lu G, Zhang ZQ, Tan Q, Zhang ZJ, Li S, Sun K, Tian L, Klahr N, Liu Y. 2008. Disrupted Frontal Connections in Band Heterotopia Mapped by Diffusion Tensor Tractography. Clinical. Neuroradiology. 18:231–236.

Mai R, Tassi L, Cossu M, Francione S, Lo Russo G, Garbelli R, Ferrario A, Galli C, Taroni F, Citterio A, et al. 2003. A neuropathological, stereo-EEG, and MRI study of subcortical band heterotopia. Neurology. 60:1834–1838.

McVea DA, Mohajerani MH, Murphy TH. 2012. Voltage-sensitive dye imaging reveals dynamic spatiotemporal properties of cortical activity after spontaneous muscle twitches in the newborn rat. J Neurosci. 32:10982–10994.

Pinard J, Feydy A, Carlier R, Perez N, Pierot L, Burnod Y. 2000. Functional MRI in double cortex: functionality of heterotopia. Neurology. 54:1531–1533.

Pizzo F, Roehri N, Catenoix H, Medina S, McGonigal A, Giusiano B, Carron R, Scavarda D, Ostrowsky K, Lepine A, et al. 2017. Epileptogenic networks in nodular heterotopia: a stereoelectroencephalography study. Epilepsia. 58:2112–2123.

Porter LL, White EL. 1983. Afferent and efferent pathways of the vibrissal region of primary motor cortex in the mouse. J Comp Neurol. 214:279–289.

Richardson MP, Koepp MJ, Brooks DJ, Coull JT, Grasby P, Fish DR, Duncan JS. 1998. Cerebral activation in malformations of cortical development. Brain. 121(Pt 7):1295–1304.

Sahu S, Buhler E, Chauvin Y, Represa A, Manent JB A model of bilateral subcortical band heterotopia created by in utero electroporation with a triple electrode probe. Program No. 594.15. 2016 Neuroscience Meeting Planner. San Diego, CA: Society for Neuroscience, 2016. Online

Schottler F, Fabiato H, Leland JM, Chang LY, Lotfi P, Getachew F, Lee KS. 2001. Normotopic and heterotopic cortical representations of mystacial vibrissae in rats with subcortical band heterotopia. Neuroscience. 108:217–235.

Shafi MM, Vernet M, Klooster D, Chu CJ, Boric K, Barnard ME, Romatoski K, Westover MB, Christodoulou JA, Gabrieli JD, et al. 2015. Physiological consequences of abnormal connectivity in a developmental epilepsy. Ann Neurol. 77:487–503.

Shepherd GM, Pologruto TA, Svoboda K. 2003. Circuit analysis of experience-dependent plasticity in the developing rat barrel cortex. Neuron. 38:277–289.

Shepherd GM, Svoboda K. 2005. Laminar and columnar organization of ascending excitatory projections to layer 2/3 pyramidal neurons in rat barrel cortex. J Neurosci. 25:5670–5679.

Spreer J, Martin P, Greenlee MW, Wohlfarth R, Hammen A, Arnold SM, Schumacher M. 2001. Functional MRI in patients with band heterotopia. Neuroimage. 14:357–365.

Szczurkowska J, Cwetsch AW, dal Maschio M, Ghezzi D, Ratto GM, Cancedda L. 2016. Targeted in vivo genetic manipulation of the mouse or rat brain by in utero electroporation with a triple-electrode probe. Nat Protoc. 11(3):399–412.

Tassi L, Colombo N, Cossu M, Mai R, Francione S, Lo Russo G, Galli C, Bramerio M, Battaglia G, Garbelli R, et al. 2005. Electroclinical, MRI and neuropathological study of 10 patients with nodular heterotopia, with surgical outcomes. Brain. 128:321–337.

Tiriac A, Del Rio-Bermudez C, Blumberg MS. 2014. Self-generated movements with "unexpected" sensory consequences. Curr Biol. 24:2136–2141.

Trotter SA, Kapur J, Anzivino MJ, Lee KS. 2006. GABAergic synaptic inhibition is reduced before seizure onset in a genetic model of cortical malformation. J Neurosci. 26:10756–10767.

Tyvaert L, Hawco C, Kobayashi E, LeVan P, Dubeau F, Gotman J. 2008. Different structures involved during ictal and interictal epileptic activity in malformations of cortical development: an EEG-fMRI study. Brain. 131:2042–2060.

Valton L, Guye M, McGonigal A, Marquis P, Wendling F, Regis J, Chauvel P, Bartolomei F. 2008. Functional interactions in brain networks underlying epileptic seizures in bilateral diffuse periventricular heterotopia. Clin Neurophysiol. 119: 212–223.

Villani F, Vitali P, Scaioli V, Rodriguez G, Rosa M, Granata T, Avanzini G, Spreafico R, Angelini L. 2004. Subcortical nodular heterotopia: a functional MRI and somatosensory evoked potentials study. Neurol Sci. 25:225–229.

Vitali P, Minati L, D'Incerti L, Maccagnano E, Mavilio N, Capello D, Dylgjeri S, Rodriguez G, Franceschetti S, Spreafico R, et al. 2008. Functional MRI in malformations of cortical development: activation of dysplastic tissue and functional reorganization. J Neuroimagidalthe posteromedial barrel subfield. J Comp Neurol. 175:455–482.

Watrin F, Manent JB, Cardoso C, Represa A. 2015. Causes and consequences of gray matter heterotopia. CNS Neurosci Ther. 21:112–122.

Wennberg R, McAndrews MP, Mikulis D. 2004. Functional imaging of the double cortex. Can J Neurol Sci. 31:254–256.

White EL, DeAmicis RA. 1977. Afferent and efferent projections of the region in mouse SmL cortex which contains the posteromedial barrel subfield. J Comp Neurol. 175:455–482.

Zhu WJ, Roper SN. 2000. Reduced inhibition in an animal model of cortical dysplasia. J Neurosci. 20:8925–8931.